



Effect of Internal Blast on Tunnel Lining and Surrounding Soil

M. D. Goel¹ · Shivani Verma² · Sandeep Panchal²

Received: 6 May 2020 / Accepted: 10 August 2020 / Published online: 25 August 2020
© Indian Geotechnical Society 2020

Abstract With the recent increase in terrorist attacks on the structures with strategic importance, detailed research intervention is required to study their behaviour under extreme loadings such as loading resulting from blast. Hence, in this investigation, three different cross sections of the tunnel with two different soil mediums are investigated under the blast loading. Herein, 3-dimensional non-linear finite element analysis of tunnels is carried out using ABAQUS/Explicit[®]. Stress–strain response of soil, concrete and reinforcement has been simulated using Mohr–Coulomb plasticity, concrete-damaged plasticity and Johnson–Cook plasticity material models, respectively. In this study, FE analysis is carried out to compare the damage of tunnel and surrounding soil under three different cross sections of tunnel, i.e. arched, circular and rectangular, and two soil conditions, i.e. saturated and unsaturated soil. Further, tunnel is analysed for an explosion of 100-kg TNT explosive placed at the centre of the cross section of tunnel. Response of the tunnels in terms of displacement and stress at critical locations is computed for the comparison of the results. Results indicate that the variation in cross-sectional shape and surrounding soil affects the behaviour of tunnel for the same amount of the explosive. It has been also observed that displacement in tunnel lining and soil surface is of smaller magnitude for

saturated soil. Also, lower stress is observed for saturated soil for all other conditions being same.

Keywords Blast loading · Numerical simulation · ConWep · Saturated and unsaturated soil mass · ABAQUS/Explicit[®]

Introduction

As availability of ground surface area has reduced for the construction of transport structure, only option available is to go underground. Under this scenario, urban cities largely depend on underground tunnels for its transport. Underground tunnels can be used for railways, roadways, water transportation, sewer lines, electrical power, routing steam or cables for telecommunication, along with connecting buildings for expedient movement of people and essential goods.

Internal explosion can lead to multiple reflection phenomenon which can be more disastrous than the external explosion as destruction is more in case of internal explosion as compared to the external blast due to reason mentioned earlier, since performing experimental blast tests would not be feasible from socioeconomic point of view. Thus, numerical and analytical study of structures exposed to blast loading is highly important and can be successfully simulated using advanced FE software. Herein, ABAQUS/Explicit[®] [1] is used for the numerical analysis of tunnel models considered.

In the literature, impact of explosive on underground structure has been investigated by many researchers [2–12]. Choi et al. [2] explained impact of explosion on facilities under the ground with respect to weight of charge, shape and size of tunnel, standoff distance and with

✉ M. D. Goel
mdgoel@apm.vnit.ac.in

¹ Department of Applied Mechanics, Visvesvaraya National Institute of Technology (VNIT), Nagpur, Maharashtra 440 010, India

² Department of Mining Engineering, Visvesvaraya National Institute of Technology (VNIT), Nagpur, Maharashtra 440 010, India

different surrounding ground condition, and it was concluded that blast wave parameters are primary function of amount of charge exploded and size of the tunnel. Liu [3] studied the dynamic analysis of subway structure under blast load and explained that the ground condition and burial depth of tunnel have a significant effect on lining stress and damage. Later on, Yang et al. [4] presented dynamic behaviour of metro tunnel for the case of ground explosion. In year 2015, Koneshwaran et al. [5] studied the performance of buried tunnel for surface blast considering fluid–structure interaction. Next year, Prasanna and Boominathan [6] carried out parametric analysis by varying the surrounding soil and explosive characteristics. They concluded that concrete tunnel suffers severe damage when embedded in a clayey stratum than in a strong rock. Afterwards, Yu et al. [7] performed numerical modelling on tunnel structure and showed that response of tunnel is influenced by soil stiffness significantly than the frictional interface, and charge location has a considerable influence on tunnel behaviour. Further, most of the past modelling work, for blast loading, has been done for circular shape of the tunnel. In year 2016, Soheyli et al. [8] reported experimental and numerical studies on tunnel buried in soil and reported the effect of various parameters. Later on, Tiwari et al. [9] reported parametric study of underground tunnels with charge weight, tunnel lining thicknesses and friction angle of soil. They said that tunnel lining deformation reduces with increase in thickness of tunnel lining. Also, tunnel lining deformation and soil deformation are found to be decreased with increase in angle of friction of soil. In the same year, Mussa et al. [10] performed series of parametric test to analyse the response of tunnel to blast waves, whereas Singh et al. [11] carried out seismic analysis of Delhi underground metro tunnel.

In previous studies, it has been observed that the analysis of blast loading was mostly restricted to circular shape of tunnel and the parametric studies have not been performed much. Hence, the present work deals with the analysis of three different shapes of the tunnels under two different soil condition, i.e. saturated and unsaturated soil. Further, behaviour of three tunnel cross section is compared in terms of displacement and von-Mises stress-time history under 100-kg TNT explosive.

Finite Element (FE) Modelling and Blast Loading

FE Model and Model Geometry

The three-dimensional FE model of the tunnel in soil is developed using explicit algorithm-based software ABAQUS/Explicit[®] [1]. A 20-m-long tunnel with three different cross sections is modelled in surrounding soil with RC

lining of thickness 300 mm. Crown of tunnel lining is at 10 m depth from ground surface, and this a typical scenario for a metro tunnel. The reinforcement, in the present study, is modelled with bars of 10 mm diameter in transverse and longitudinal directions, and transverse reinforcement is arranged at 300 mm spacing for circular and rectangular tunnels and 322 mm spacing for arched tunnel to account for geometry effect. The spacing and number of reinforcement are typical in such linings, and the same is adapted in this study from earlier work of Tiwari et al. [9]. Further, reinforcement spacing and number of bars are arrived by considering the same percentage of reinforcement for all the cases considered herein. A total of 20 number bars are used as longitudinal reinforcement and are placed around the perimeter of the transverse reinforcement. The hoop reinforcement is provided as double-layered reinforcement with a distance of 120 mm in between them. The tunnel is placed in a soil media of length 20 m with 26 m × 26 m, 26 m × 24.7 m and 26 m × 25.34 m cross section for circular, rectangular and arched tunnel, respectively. Since the depth of tunnel burial is 10 m and the cross section of tunnel considered here is of different shapes, hence to make soil media constant surrounding the tunnel lining, the dimensions of soil domain for all shapes considered are varied. It is important to mention that nonreflecting boundary conditions are applied on the outer boundary to avoid reflection of blast wave from the soil interfaces. This boundary condition reflects that soil boundary is sufficiently large and it is not contributing any reflection from the surface. Considering this, total domain of investigation is arrived upon. Finite element mesh and geometry of soil, lining of tunnel and reinforcement and complete model are shown in Fig. 1a–d, respectively. Finite element models for soil and reinforced concrete lining are developed as three-dimensional solid deformable part in ABAQUS/Explicit[®] with element specification as reduced integration, eight-noded brick elements with hourglass and distortion control (i.e. C3D8R element).

Tunnel lining and soil near to lining are meshed with higher-density mesh based on mesh convergence study (Fig. 1d). The reinforcement bars are embedded in concrete lining and modelled with beam element of two nodes (i.e. B31 element). Proper connection between concrete and reinforcement bars is created with the help of embedded constraints option of ABAQUS/Explicit[®] [1]. The contact between surrounding soil and tunnel lining is modelled with surface to surface contact available in ABAQUS/Explicit[®] [1]. For contact definition in normal direction, hard contact is chosen, and in tangential direction, frictional contact with a penalty of 0.2 is adopted for the study. The location of explosion inside the tunnel and location of points considered for the parametric study are shown in Fig. 2a and b, respectively. Point 1 is top node of

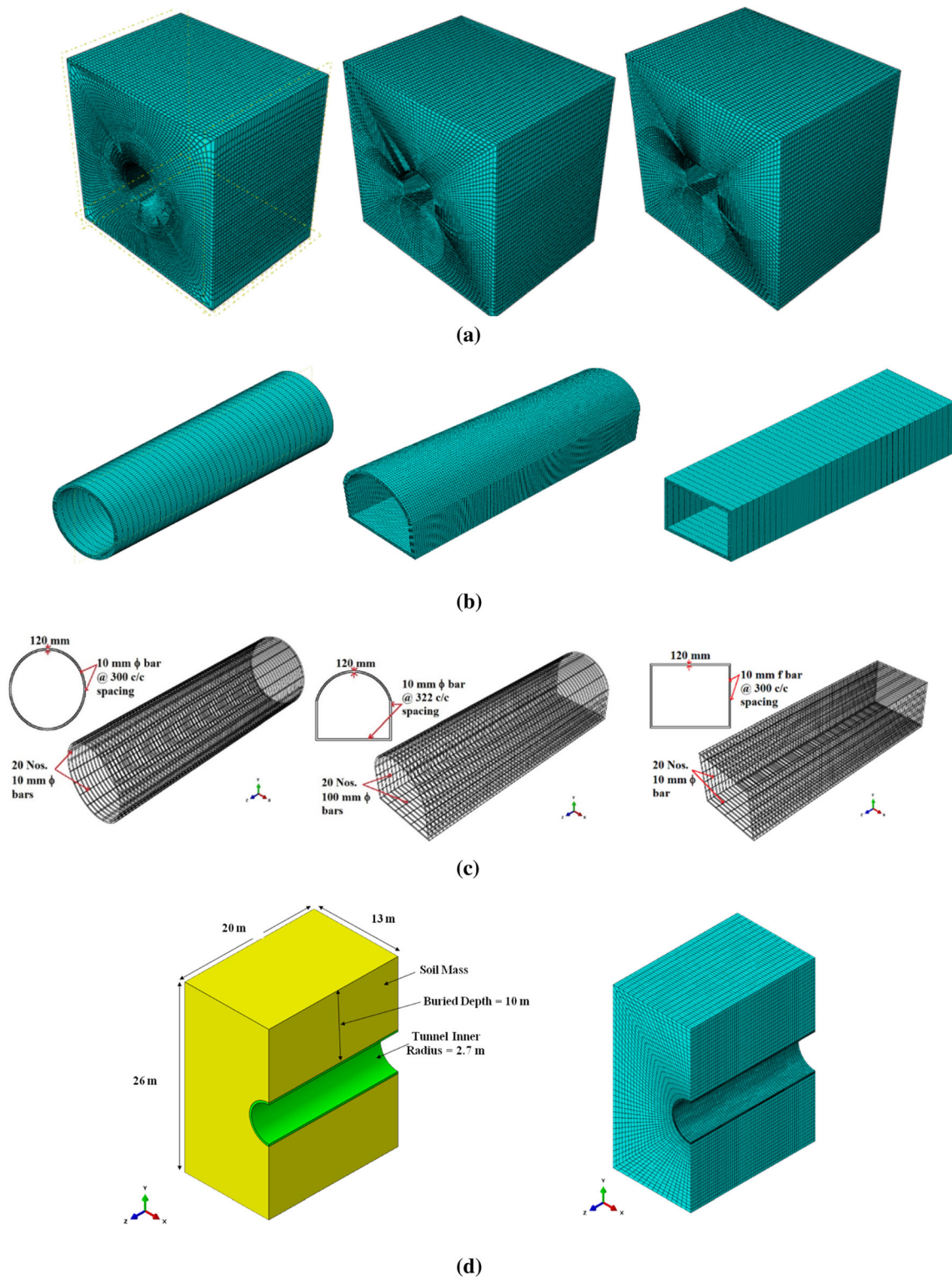


Fig. 1 Details of mesh for circular, arched and rectangular tunnels for **a** soil media **b** tunnel lining and **c** reinforcement and **d** complete model with tunnel lining and soil mass and its mesh of various elements of model

the crown of tunnel lining, and point 2 is the middle node on the ground surface.

Mesh convergence study has also been performed considering three different element sizes designated as coarse, medium and fine mesh (Fig. 2c). Based on this mesh

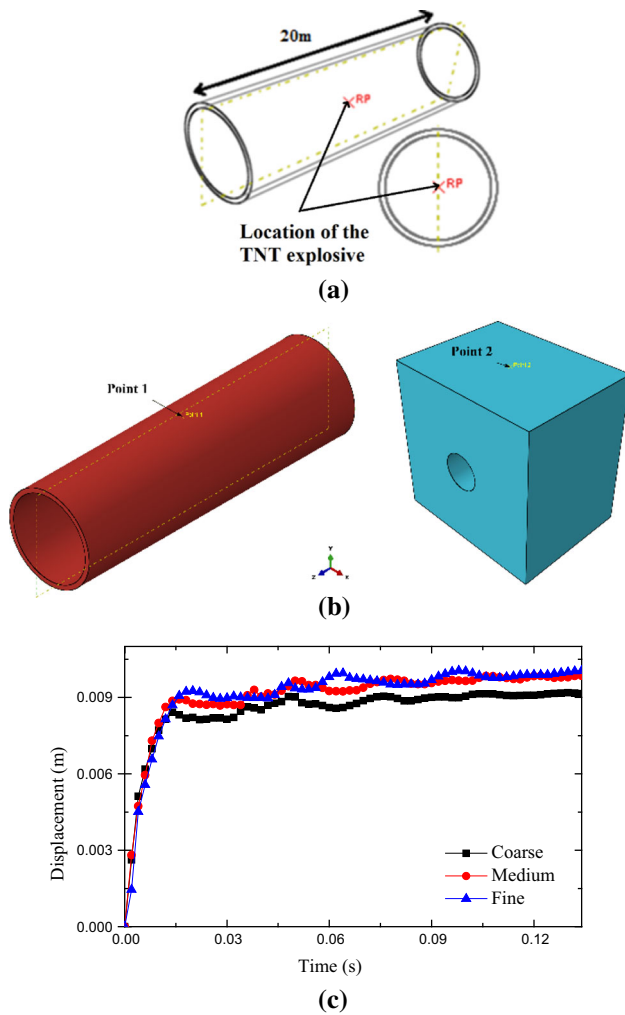


Fig. 2 **a** Location of the TNT explosive, **b** locations of the observation points considered for the parametric study and **c** mesh convergence study of the tunnel

convergence study, fine mesh is adopted for all other analysis. In addition to this, mesh size for the soil domain is adopted accordingly to create fine mesh around the tunnel lining and then increased to medium mesh as the distance increases from the tunnel to reduce the computational cost without affecting the results. This methodology is adapted to reduce the computational time and cost as our main interest is deformation of the tunnel lining.

Blast Loading

For the current study, TNT explosive of 100 kg is considered at the centre of the tunnel. Blast loading is performed with the help of ConWep tool available in ABAQUS/Explicit® [1]. The equation for blast load calculation used in ConWep tool is developed by Kingery and Bulmash [12]. The equation used in the ConWep model is represented as follows:

$$p(t) = p_i(t)(1 + \cos \theta - 2 \cos^2 \theta) = p_r \cos^2 \theta \quad \text{if } \cos \theta \geq 0, \tag{1}$$

$$p(t) = p_i(t) \quad \text{if } \cos \theta < 0 \tag{2}$$

where $p(t)$ is combined pressure depending on the angle (say θ) at which the shock impinges on the surface, $p_i(t)$ is the incident pressure, and $p_r(t)$ is the reflected pressure.

Material Model and Properties

Material Model and Properties of Concrete

Concrete in tunnel lining is modelled with M50 grade by utilising concrete damage plasticity (CDP) model available in ABAQUS/Explicit® [1]. The stress–strain correlation of concrete damage plasticity model is expressed by,

$$\sigma_t = (1 - d_t)D_0^{el} : (\varepsilon - \varepsilon_t^{pl}) \tag{3}$$

$$\sigma_c = (1 - d_c)D_0^{el} : (\varepsilon - \varepsilon_c^{pl}) \tag{4}$$

where t and c here show tension and compression behaviour of concrete, respectively. Here, σ_t and σ_c represent tensile and compressive stress vectors, respectively; ε_t^{pl} and ε_c^{pl} represent plastic strains; d_t and d_c represent damage variables which considerably are corollaries of plastic strain; D_0^{el} is initial elastic modulus with undamaged condition. The yield function of CDP model and material properties of concrete are taken from Jankowiak and Lodygowski [13]. Stress–strain characteristic curves of concrete under compression and tension and damage behaviour of concrete in compression and tension are used in the study. The Young’s modulus is 35.36 GPa, Poisson’s ratio = 0.19, density = 2400 kg/m³ with a dilatancy angle of 38°. Further, the eccentricity, f_{bo}/f_{co} ratio and k values are 1, 1.12 and 0.67, respectively [13].

Material Model and Properties for Reinforcement Bars

The stress–strain behaviour of reinforcement bars has been modelled with Johnson–Cook (J–C) model [14]. The stress (σ)–strain (ε) relationship of J–C model for the dynamic loading is expressed as [14]:

$$\sigma = (A + B\varepsilon^n) (1 + C \log \dot{\varepsilon}^*) (1 - T^m) \tag{5}$$

where ε^* represents plastic strain; $\varepsilon^* = \dot{\varepsilon}/\dot{\varepsilon}_0$ for which $\dot{\varepsilon}$ shows equivalent plastic strain rate and $\dot{\varepsilon}_0 = 1/s$ shows reference strain rate. In the above equation A , B , C , m and n are the model parameters; T^* represents homologous temperature. The steel considered for reinforcement in lining is of grade Fe-415. Material properties used for steel

have density of 7800 kg/m³, yield strength of 415 MPa, Young’s modulus of 200 GPa, Poisson’s ratio as 0.3 and strain rate of 100/s. Strain rate-dependent J–C model is used here, and material constants are achieved with the help of mechanical testing and used in the present study for the strain rate of 100/s. The values of the material constants are as follows: $A = 360$ MPa, $B = 635$ MPa, $n = 0.114$, $C = 0.075$ [15].

Material Model and Properties for Soil

Mohr–Coulomb plasticity model is used herein for the soil surrounding the tunnel. In Mohr–Coulomb criterion, it is assumed that failure depends on maximum shear stress and shear stress at failure is affected by normal stress. The above statement can be expressed by constructing a Mohr’s circle for failure states of stress considering maximum and minimum principal stresses. The failure line of Mohr–Coulomb is nearly the straight line which touches the Mohr’s circles (Fig. 3). Therefore, Mohr–Coulomb model is defined as,

$$\tau = c \pm \sigma \tan \phi \tag{6}$$

where τ represents shear stress, σ represents normal stress, c represents cohesion of the material, and ϕ expresses the friction angle of material. From Mohr’s circle, shear stress, τ , and normal stress, σ , are represented by,

$$\tau = c \pm \sigma \tan \phi \tag{7}$$

$$\tau = s \cos \phi \tag{8}$$

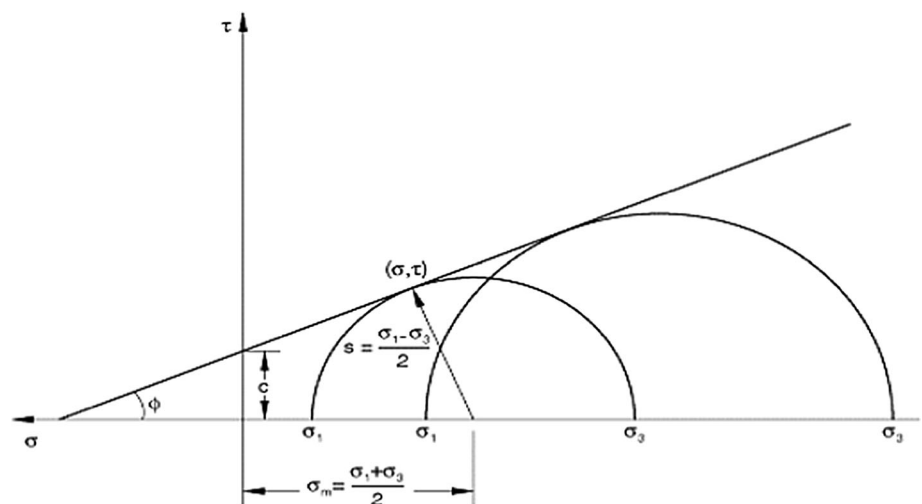
$$\sigma = \sigma_m + s \sin \phi \tag{9}$$

Hence, using values of τ and σ , Mohr–Coulomb model can be rewritten as,

$$s + \sigma_m \sin \phi - c \cos \phi = 0 \tag{10}$$

$$s = 0.5(\sigma_1 - \sigma_3) \text{ and } \sigma_m = 0.5(\sigma_1 + \sigma_3) \tag{11}$$

Fig. 3 Mohr–Coulomb yield model for soil used in the present study



where σ_1 is the maximum principal stress, and σ_3 is minimum principal stress. Further, properties of the saturated soil used in this analysis include Young’s modulus = 40 MPa, Poisson’s ratio = 0.49, cohesion = 50 kPa, friction and dilatancy angle = 0°. For unsaturated soil, these properties are 50 MPa, 0.30, 90 kPa, 20° and 0°, respectively [16].

Validation of the Present Finite Element Scheme

To confirm the validity of the current numerical simulation, results of present ABAQUS/Explicit[®] simulation of concrete slab subjected to blast loading are validated with the experiment results reported by Li et al. [17]. They performed experimental test on a plain concrete slab with 1.2 m × 0.8 m × 0.12 m dimensions, and authors numerically analysed the same using ABAQUS/Explicit[®] with all material, geometrical and blast loading condition being same as reported by Li et al. [17]. In this validation, M25 grade of concrete is used to model the concrete slab along with concrete damage plasticity material model. Finite element model for concrete slab is developed as three-dimensional solid deformable part in ABAQUS/Explicit[®] with element specification as reduced integration, eight-noded brick elements with hourglass and distortion control (i.e. C3D8R element). The mesh size of 10 mm is considered for the concrete slab. The geometry, meshing detail and location of blast are same as reported by Li et al. [17]. The slab is subjected to blast load of centrally located 8-kg TNT at a standoff distance of 1.5 m. ConWep tool is used for the numerical simulation of blast, wherein boundaries are fixed in three Cartesian coordinates, i.e. x , y and z . Displacement at the centre of the slab is compared for the validation of the present FE scheme with the experimental results reported by Li et al. [17]. The damage

of the concrete slab in experimental test and numerical results is shown in Fig. 4. It can be seen from Fig. 4 that the damage profile of the experimental and numerical results is of similar nature. The peak deflection value for the slab from the experimental is reported as 190 mm, whereas, from the present numerical simulation, the peak deflection is found to be 180.6 mm. The error in the peak deflection from the present numerical study and experimental results reported by Li et al. [17] is found to be 4.94%. This is an acceptable error considering the FE analysis, and hence, the present numerical scheme is considered to be validated.

Further, for improved confidence, another validation is carried out using the experimental results reported by Soheyli et al. [8]. Herein, a box-shaped tunnel of length 4 m, cross section of 1 m \times 1 m and wall thickness of 100 mm is subjected to explosion of 1.69-kg TNT located at a lateral distance of 4 m from the tunnel exterior face. Explosive is buried 2 m below the ground surface. The experiment setup is numerically modelled, and comparison is made based on acceleration and displacement on vertical wall of tunnel along its length as shown in Fig. 5a and b. The results obtained from numerical simulation agree well with experimental results provided by Soheyli et al. [8], thus confirming the validity of the present numerical scheme.

Results and Discussion

Herein, FE simulation of tunnel in surrounding soil mass exposed to internal blast load has been performed for three different cross-sectional shapes. The effect of 100-kg TNT explosive has been considered for the parametric study of surrounding soil and tunnel lining. Here, values of displacement are considered to be positive in the positive x , y and z coordinates. Although blast explosion is very short-duration phenomenon, time period of 150 ms is considered to see stability of tunnel lining and surrounding soil over a period of time.

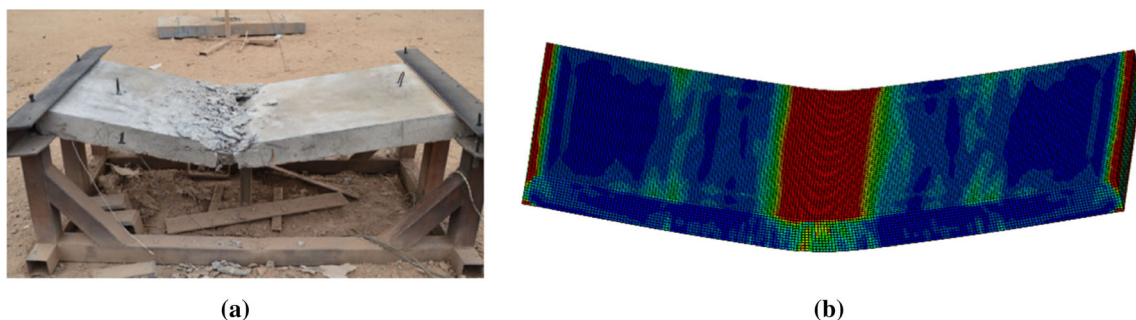


Fig. 4 Damage in the concrete Slab **a** Experimental test as per Li et al. [17]. **b** Present numerical modelling

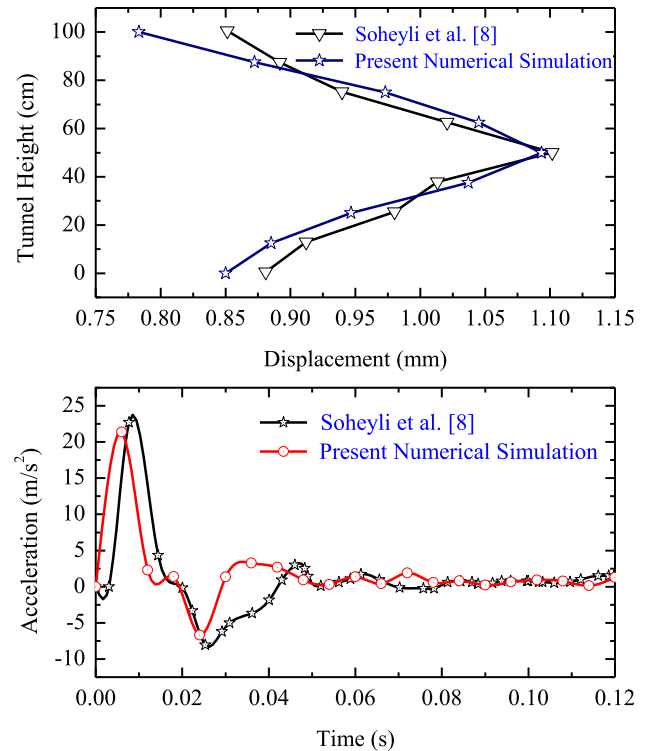


Fig. 5 Validation using Soheyli et al. [8] experimental results with the present numerical scheme

Displacement and Stresses in RC Lining

The point on the crown of tunnel lining considered for the current parametric study is shown in Fig. 2. Displacement on the crown node of tunnel cross section is considered for the analysis. In the present work, it is observed that tunnel in saturated soil is experiencing lower peak displacement than that of the tunnel in unsaturated soil. The intensity of blast wave is of lower magnitude in unsaturated soil as compared to saturated soil, but displacement of unsaturated soil is found to be of higher magnitude because of weak bond between soil particle and skeleton of soil. It is also known that unsaturated soil has large volume of air which causes high compressibility. Variation of displacement

with time for three different cross sections of the tunnel is shown in Fig. 6.

It can be observed from these results that displacement variation for unsaturated soil is more fluctuating because of more voids. Since elastic modulus of unsaturated soil is higher, it is experiencing smaller strain values as compared to the saturated soil condition. From the results, it is found that tunnel with arched and rectangular lining is experiencing 29.56% and 50.31%, respectively, more displacement than the circular lining on top node of the tunnel lining with all other parameters being same.

It can also be seen that at time, $t = 0.01$ s, there is a second peak of displacement and after that the displacement continues to be constant. This can be explained through Fig. 7, which shows the velocity profile for the node considered on the tunnel lining. Since the point considered on the top node of the lining and the soil ground surface is left free, soil surface reflects the shock wave once reached to it. When the reflected waves reach to the tunnel lining, again it causes the velocity to increase, but the magnitude will be lesser as most of the shock waves get dissipated while travelling to surface and then back to the tunnel lining. This rebound in the velocity causes the increases in the displacement in the tunnel lining. From Fig. 6 it can be seen that tunnel with rectangular shape is experiencing the maximum displacement for both saturated and unsaturated soil conditions, whereas tunnel with circular shape is experiencing the least displacement amongst all the shapes. The behaviour of the arched shape tunnel is

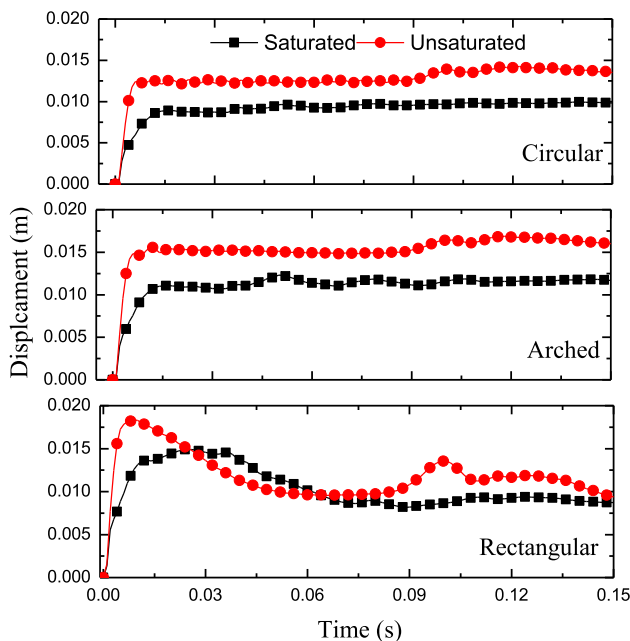


Fig. 6 Variation of displacement with time for the top middle node of circular, arched and rectangular tunnel lining for two soil condition

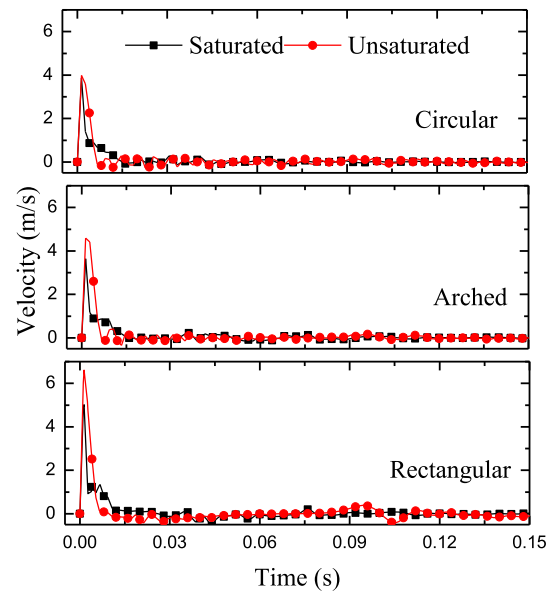


Fig. 7 Variation of velocity with time for the top middle node of circular, arched and rectangular tunnel lining for two soil condition

similar as that of the circular tunnel but with greater values of displacement for both soil conditions.

Figure 8 represents the von-Mises stress–time history profiles for all parameters considered in the current study. The stress developed in the tunnel lining is more for unsaturated soil as compared to the saturated soil condition because internal friction angle and cohesion of surrounding soil are more for unsaturated soil. It is seen from this figure that tunnel is experiencing fewer fluctuations in stresses when the soil is saturated for all shapes of the tunnel under consideration because of the smaller voids between the soil

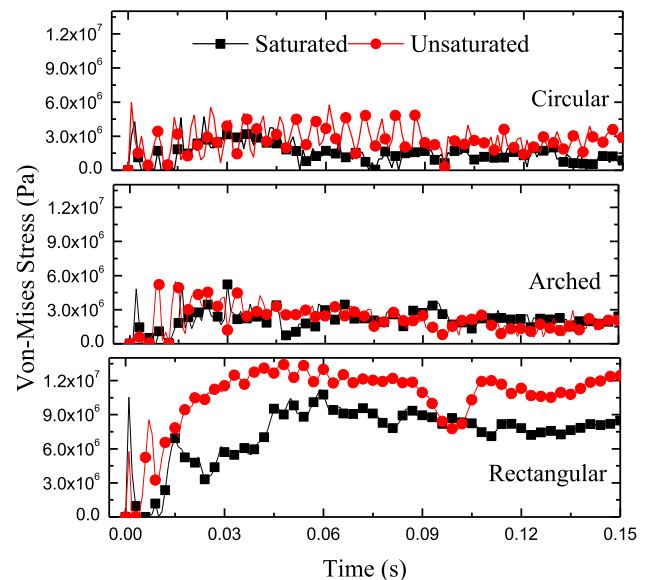


Fig. 8 Von-Mises stresses-time history at crown of the tunnel lining for circular, arched and rectangular tunnel

particles. This decrease in the voids is because of the increase in density of saturated soil. Since the wave velocity is the inverse function of density and direct function of stress, it can be said that with greater velocity and lower density, the unsaturated soil is experiencing the stresses with higher magnitude. And soil with saturated condition has experienced the lower stresses for all cross-sectional shapes. Further, it is found that tunnel with arched and rectangular lining experiences 18.28% and 138.61%, respectively, more stresses than circular lining on top node of the tunnel lining keeping all other parameters constant. Peak displacement and peak stress values for all points under consideration for tunnel lining are summarised in Table 1. From Fig. 7, it can be seen that the velocity for rectangular tunnel is highest and velocity for circular tunnel is least amongst all shapes of tunnel, for both saturated and unsaturated soil.

The first peak of the stress is governed by the standoff distance, whereas the reflected peaks of the tunnel lining are governed by both standoff distance and the exposed shape of lining towards the blast location. The fluctuations of stress in the tunnel lining can be explained with the help of velocity profile as shown in Fig. 7. It can be seen from Figs. 7 and 8 that for higher reflected velocity the developed von-Mises stresses are of greater magnitude. In addition to above, for rectangular tunnel, mean stress after the peak stress is quite high as compared to the other two cross sections of tunnel considered herein. In Fig. 8, von-Mises stress-time history is shown and it can be seen from this figure that the magnitude of stress is increased up to some time period; then, it becomes constant. These constant stresses are the residual stresses, and the initial increase in the magnitude of stresses is because of the reflected waves, which is explained earlier in this section.

Displacement and Stress in Soil

The point on the ground surface considered for the current parametric study is shown in Fig. 2. Top middle node on the soil is considered for the comparison of the results. As the density of saturated soil is higher than that of the unsaturated soil, wave in saturated soil reaches the soil

surface earlier than that in case of unsaturated soil. It has been seen that saturated soil has experienced lower displacement than that of unsaturated soil. Further it has been found that soil surface experienced lower magnitude of displacement when tunnel lining is circular as compared to other two shapes. Here, soil with rectangular and arched lining is experiencing 25.92% and 23.49% more displacement than soil with circular lining. Displacement–time variation for the soil is shown in Fig. 9.

It can be seen from Fig. 9 that peak displacement occurs after a certain time delay because of the buried depth. The first ever peak of displacement occurs in case of rectangular shape, and the reason behind this is highest velocity for the same. The velocity generated at time, $t = 0.049$ s, is of magnitude 0.846 m/s, 0.865 m/s and 1.086 m/s for circular, arched and rectangular shape, respectively, for unsaturated soil and for saturated soil lesser velocity is experienced for all shapes under consideration. Figure 10 shows the von-Mises stress variation with time for the soil. Small voids in case of saturated soil are the reason for less fluctuation on the surface of soil as compared to the unsaturated soil. It has been seen that blast wave generated by the explosion is taking less time to reach the ground surface in case of saturated soil because of higher density.

It has been also seen that the magnitude of stress developed is more when the soil is unsaturated as compared to the saturated soil. As it can be seen earlier that higher magnitude of velocity leads to the generation of higher stresses in case of unsaturated soil, whereas for saturated soil the developed stresses are of lower magnitude as the velocity is also less for the same. From Fig. 10 it can be seen that the highest stresses are developed in case of rectangular shape as the wave velocity is maximum for the same, whereas stress developed in arched and circular shape is of equivalent magnitude for unsaturated soil, as the velocity is approximately of similar magnitude.

The rebound in the stress is because of the reflection of the wave for all considered cases. As it can be seen that the magnitude of second, third and fourth peak is decreased with time, which is because the magnitude of reflected wave also decreases. Most of the energy gets absorbed after every reflection of wave and after the full dissipation of

Table 1 Displacement and stresses at critical points for tunnel lining

Tunnel shape	Peak displacement at tunnel (mm)		Peak von-Mises stress (MPa) in soil	
	Unsaturated soil	Saturated soil	Unsaturated soil	Saturated Soil
Circular	13.90	9.93	5.97	4.70
Arched	16.86	12.86	5.47	5.56
Rectangular	18.30	14.92	13.56	11.21

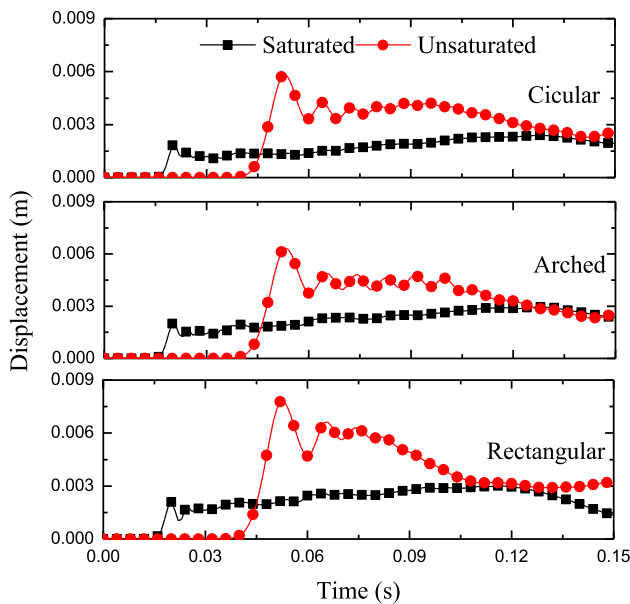


Fig. 9 Displacement–time history on the top middle node considered on the surface of the soil for circular, arched and rectangular tunnel

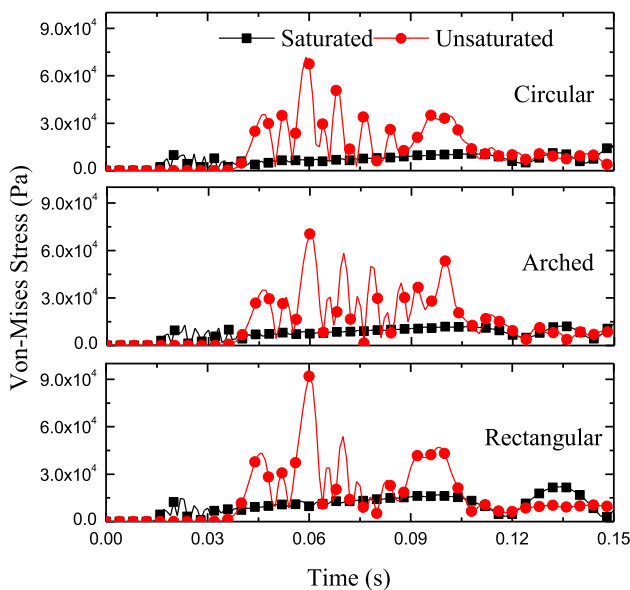


Fig. 10 von-Mises stresses on the surface of the soil for circular, arched and rectangular tunnel

wave the residual deflection is left, which is or very smaller magnitude. Nodal values for displacement and stresses for points under consideration on surface soil are summarised in Table 2.

Conclusions

In this study, analysis of underground tunnel exposed to internal blast loading with surrounding media as soil is carried out. It includes dynamic assessment of tunnel lining and soil for various tunnel cross-sectional shapes using explicit algorithm-based software, i.e. ABAQUS/Explicit®. Here, soil media and reinforced concrete are modelled with Lagrangian elements. Based on parametric study, the following observations are obtained from the current study

1. For the tunnel shapes considered in this study, it has been found that tunnels buried in the saturated soil and ground surface has experienced lower displacement as compared to the unsaturated soil condition. This shows that the surrounding media affect the stability of the underground tunnel considerably. It has also been observed that the tunnel with circular shape is most resistant to the blast loading as compared to the other tunnel shapes considered in this study.
2. Stresses developed in the tunnel lining and soil surface are of higher magnitude in case of unsaturated soil for all the shapes considered in this study. Stress fluctuation also leads to the instability of soil medium. The stresses developed for the rectangular lining are of higher magnitude for both the case of soil medium considered herein.
3. The wave reaches to ground earlier in saturated soil than that of the unsaturated soil, but the magnitude of the wave in unsaturated soil is higher than that of the saturated soil. Hence, the ground surface displacement is higher for unsaturated soil as compared to that of the saturated soil.

From the above discussion, it can be said that surrounding soil and the shape of the tunnel considerably affect the stability of the tunnel lining and the ground surface.

Table 2 Displacement and stresses values at the top middle node on the surface of soil

Tunnel shape	Peak displacement (mm) Unsaturated soil	Peak displacement (mm) Saturated soil	Peak von-Mises stress (kPa) Unsaturated Soil	Peak von-Mises stress (kPa) Saturated soil
Circular	5.83	2.39	71.82	16.08
Arched	6.34	2.95	70.41	13.83
Rectangular	7.80	3.01	91.75	22.07

References

1. ABAQUS, Explicit® (2018) User's manual. Dassault Systemes Simulia Corporation, Paris
2. Choi S, Wang J, Munfakh G, Dwyre E (2006) 3D nonlinear blast model analysis for underground structures. In: *GeoCongress 2006: geotechnical engineering in the information technology age*, pp 1–6
3. Liu H (2009) Dynamic analysis of subway structures under blast loading. *Geotech Geol Eng* 27(6):699. <https://doi.org/10.1007/s10706-009-9269-9>
4. Yang Y, Xie X, Wang R (2010) Numerical simulation of dynamic response of operating metro tunnel induced by ground explosion. *J Rock Mech Geotech Eng* 2(4):373–384. <https://doi.org/10.3724/SP.J.1235.2010.00373>
5. Koneshwaran S, Thambiratnam DP, Gallage C (2015) Performance of buried tunnels subjected to surface blast incorporating fluid-structure interaction. *J Perform Constr Fac* 29(3):04014084. [https://doi.org/10.1061/\(ASCE\)CF.1943-5509.0000585](https://doi.org/10.1061/(ASCE)CF.1943-5509.0000585)
6. Prasanna R, Boominathan A (2015) Numerical simulation on behaviour of concrete tunnels in internal blast loading. In: *Computer methods and recent advances in geomechanics: proceedings of the 14th international conference of international association for computer methods and recent advances in geomechanics*. Taylor & Francis Books Ltd., pp 1907–1911
7. Yu H, Wang Z, Yuan Y, Li W (2016) Numerical analysis of internal blast effects on underground tunnel in soils. *Struct Infrastruct Eng* 12(9):1090–1105. <https://doi.org/10.1080/15732479.2015.1077260>
8. Soheyli MR, Akhaveissy AH, Mirhosseini SM (2016) Large-scale experimental and numerical study of blast acceleration created by close-in buried explosion on underground tunnel lining. *Shock Vib*. <https://doi.org/10.1155/2016/8918050>
9. Tiwari R, Chakraborty T, Matsagar V (2017) Dynamic analysis of tunnel in soil subjected to internal blast loading. *Geotech Geol Eng* 35(4):1491–1512. <https://doi.org/10.1007/s40098-016-0179-5>
10. Mussa MH, Mutalib AA, Hamid R, Naidu SR, Radzi NAM, Abedini M (2017) Assessment of damage to an underground box tunnel by a surface explosion. *Tunn Undergr Space Technol* 66:64–76. <https://doi.org/10.1016/j.tust.2017.04.001>
11. Singh M, Viladkar MN, Samadhiya NK (2017) Seismic analysis of Delhi metro underground tunnels. *Indian Geotech J* 47(1):67–83. <https://doi.org/10.1007/s40098-016-0203-9>
12. Swisdak Jr MM (1994) Simplified kingery airblast calculations. Naval Surface Warfare Center Indian Head Division MD. Technical report ADA526744
13. Jankowiak T, Lodygowski T (2005) Identification of parameters of concrete damage plasticity constitutive model. *Found Civ Env Eng* 6(1):53–69
14. Johnson GR, Johnson GR (1983) A constitutive model and data for metals subjected to large strains, high strain rates and high temperatures. In: *Proceeding of 7th international symposium on ballistics*, pp 541–547
15. Goel MD, Matsagar VA, Gupta AK (2011) Dynamic response of stiffened plates under air blast. *Int J Prot Struct* 2(1):139–155. <https://doi.org/10.1260/2041-4196.2.1.139>
16. Al Amlı AS, Al-Ansari N, Laue J (2019) Study numerical simulation of stress–strain behavior of reinforced concrete bar in soil using theoretical models. *Civ Eng J* 11(5):2349–2358. <https://doi.org/10.28991/cej-2019-03091416>
17. Li J, Wu C, Hao H, Su Y, Liu Z (2016) Blast resistance of concrete slab reinforced with high performance fibre material. *J Struct Integr Maint* 1(2):51–59. <https://doi.org/10.1080/24705314.2016.1179496>

Publisher's Note Springer Nature remains neutral with regard to jurisdictional claims in published maps and institutional affiliations.